Journal of Himalayan Earth Sciences 45(1) (2012) 31-52

Mineralogy and geochemistry of diorites and associated hydrothermal sulfide mineralization of Gawuch Formation in Drosh area, Chitral, northern Pakistan

Tazeem Tahirkheli, M. Tahir Shah, M. Asif Khan and Rubina Bilqees
National Centre of Excellence in Geology, University of Peshawar, Pakistan

Abstract

Sulfide mineralization in Drosh-Shishi area is related to hydrothermal activity which is mainly associated with altered diorite and quartz veins of Gawuch Formation. This Formation comprises variably metamorphosed volcanics and sediments intruded by plutons of diorite and granodiorite composition. Three varieties of diorites are distinguished in the studied area. These include 1) diorites, 2) altered diorites and 3) gneissose diorites. All types of diorites are mineralogically similar having major constituent minerals like plagioclase, orthoclase, amphibole and quartz. Calcite, chlorite, and epidote occur as minor secondary minerals while muscovite, biotite and ore occur as accessory phases.

Detailed geochemistry, mainly based on major and trace elements, suggests that the magmatism responsible for Gawuch Formation was calc-alkaline and contains strong subduction component. Sulfide mineralization occurs in association with diorites and quartz veins, along foliation planes, as dissemination and as supergene enrichment. Tetrahedrite, chalcopyrite, pyrite and galena are dominant ore minerals with subordinate amounts of sphalerite, magnetite, malachite and azurite. Electron microprobe analyses show the pure nature of these ore phases. A variable gain and loss of MnO, K_2O, Na_2O and P_2O_5 are noticed in mineralized diorite which shows an enrichment of Cr, Zn, Mo, Cd, Ag and Au. Both mineralized diorites and mineralized quartz veins have a high $\delta^{18}O$ signature, suggesting the involvement of isotopically heavy ore forming fluid in the alteration and copper mineralization.

Keywords: Petrochemistry; Sulfide-mineralization; Gawuch Formation; Chitral

1. Introduction

The study area lies in Chitral, at the north-western margin of the Kohistan Island-arc terrain in northern Pakistan. Sulfide mineralization occurs in the Drosh Shishi area in a narrow belt of 100m width and 15 Km length in the vicinity of Shyok suture zone (Fig. 1). Lithological units like metabasalts / meta-andesites have intercalations of carbonate lithologies (limestone and marble) of Gawuch Formation (Pudsey et al., 1985) form cover sequence in this part of the Kohistan terrain. These lithologies are western equivalents of the better known Chalt-Yasin Group of Yasin and Hunza valleys (Tahirkheli and Jan, 1979; Petterson and Windley, 1991). Abundant intrusions of Early Eocene age of sills of dioritic and granodioritic composition are present in the Gawuch Formation belonging to Lowari pluton of Kohistan batholiths. Copper mineralization occurs in association with these diorites, granodiorite and associated quartz veins in Drosh-Shishi area.

Present work is aimed at detailed mineralogy, geochemistry and tectonic setting of diorites/ granodiorites to decipher the mode of copper mineralization, enrichment and depletion of major and trace elements, and the source of mineralizing fluid involved in copper mineralization.

2. Regional and local geological setting

Northern part of the Kohistan terrain comprises of three principal tectonic units, which from north to south include: 1) Shyok suture mélange, 2) sedimentary-volcano cover sequence and 3) Kohistan batholiths. The Shyok suture separates the Eurasian plate to the north from the Kohistan terrain to the south (Tahirkheli and Jan, 1979; Bard et al., 1980). Shyok suture is a razor-

sharp fault to a 4 km wide zone and consists of a melange zone comprising of lenticular blocks of highly variable lithology including serpentinites, marbles, conglomerates, sandstones and basalts, mostly set in a pellitic matrix comprising slates of turbidite nature which is known as Shyok mélange zone (Pudsey and Maguire, 1986). This forms a collision zone between Kohistan and Eurasian plates and marks the closure of the northern branch of the Neotethys, termed the Shyok ocean (Khan et al., 1989). A lenticular belt composed of volcano-sedimentary cover sequence sandwiched between the Shyok suture in the north and the Kohistan batholith in the south in Kohistan terrain. This cover sequence comprises a thick succession of metabasalts at the base (the Chalt volcanics; Petterson and windley, 1991), which is overlained by a succession of quartzites, limestones and turbidites (Pudsey et al., 1985; Pudsey and Maguire, 1986), termed as Yasin Group. The Yasin Group contains Early Cretaceous fauna and is marine in origin (Pudsey and Maguire, 1986). Khan et al. (1994) have recently identified a succession of paragneisses, schists and amphibolites called the Gilgit Formation which occupies the foot of the Chalt volcanics. The Kohistan batholith is intrusive into both of the above mentioned tectonic elements and comprises of plutons of a wide range of compositions from gabbros, through diorites, tonalities and granodiorites to granites and forms the midrib of the Kohistan terrain. The intrusions in the Kohistan batholith spans over a time range of 102 to 29 Ma (Petterson and Windley, 1986).

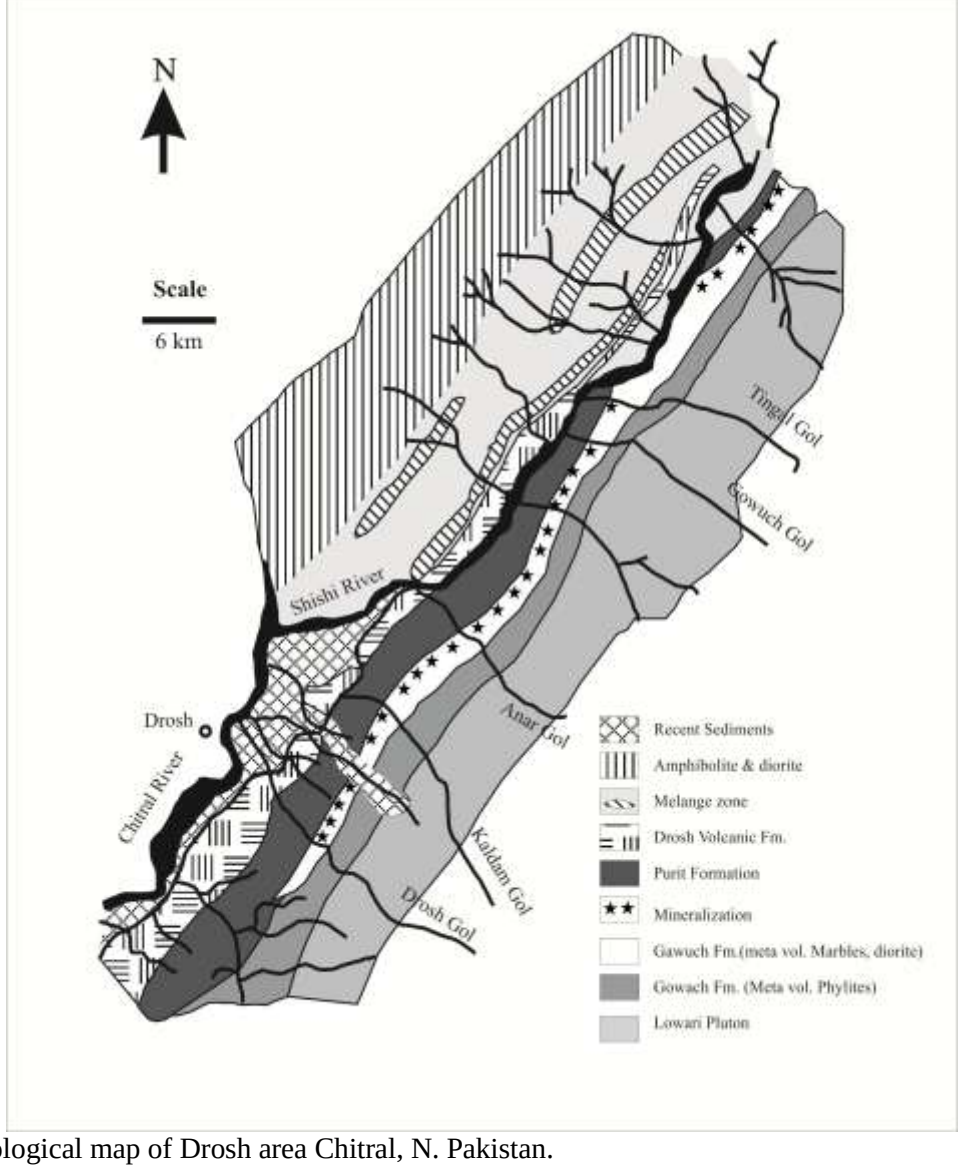

Fig. 1. Geological map of Drosh area Chitral, N. Pakistan.

The study area (Fig. 1) in Chitral comprises Drosh-Shishi area, the NW margin of Kohistan contains all the three tectonic elements outlined above. The Shyok suture consists of lenticular blocks of ultramafics, limestones etc. but the volcano-sedimentary succession in this area is, however, much more complex than that of the Yasin-Hunza segment. Pudsey et al. (1985) recognized three formations, which from north to south include 1) Drosh Formation, 2) Purit Formation and 3) Gawuch Formation. Drosh Formation comprises of a succession of andesite/dacite volcanics lying over the Purit Formation and may possibly represent a phase of Eocene volcanic event similar to that of Dir-Utror (Shah and Shervais, 1999). Purit Formation, comprising of red conglomerates, sandstones and shale, is fluvial in origin (Pudsey et al., 1985). The Gawuch Formation comprises of metabasalts and limestones and is probably marine in origin. The copper mineralization occur in the Gawuch Formation is belonging to the Kohistan batholith. The Gawuch Formation has an intrusive contact with the Lowari pluton towards south, however, the contact is now intensely sheared and is occupied by phyllites derived from metavolcanics of the Gawuch Formation through mylonitization (Tahirkheli et al., 2005). Strongly sheared metabasalts comprise much of the lower half of the Gawuch Formation and have been transformed to phyllites, whereas, the upper half of the succession consists of intercalated metabasalts and limestone/marble. Additionally, this upper part is also intruded by sills of diorite and granodiorite composition which are themselves pervasively intruded by quartz veins.

A thick layer of marble is occupying the contact between the Gawuch and the Purit formations. Copper mineralizatoin in the Gawuch Formation has been identified in the field: 1) copper mineralization along quartz veins, 2) copper mineralization along foliation planes, 3) disseminated copper mineralization and 4) supergene enrichment of copper (Tahirkheli et al., 1997). The contact between the Gawuch Formation and the overlying Purit Formation is occupied by a 10 m thick band of marble.

3. The Drosh diorite complex

3.1. Petrography

The diorites of the studied area are medium- to coarse-grained, equigranular to inequigranular, subhedral characterized by a common hypediomorphic granular texture. The major constituent minerals are plagioclase, orthoclase, amphibole and quartz. Calcite, chlorite, epidote occur as minor constituents, muscovite, biotite and ore are accessory minerals. All rocks are slightly foliated. Granulation is developed along margins.

Altered diorites are mineralogically similar to the fresh diorites and granodiorites, but are different in texture. The principal difference, however, is the degree of alteration. The altered diorites are fine-to coarse-grained, inequigranular and are characteristically porphyritic, but some rocks show typically idiomorphic porphyritic and poikilitic textures. Feldspar and quartz occur as primary minerals, sphene and ore as accessory while chlorite, epidote, sericite and calcite occur as secondary minerals. At places relicts of hornblende are also present in the aggregate of chlorite.

Most of the diorites are strongly foliated and have a banded appearance in the hand specimen. Some of the samples are prophyroclastic with eye-shape appearance of feldspar grains set in a matrix of fine-grained dynamically recrystallized matrix. As far as the mineral composition is concerned, there are only subtle differences between these and non-foliated diorites described above. The major constituents of diorite gneisses are plagioclase and quartz. Amphibole, chlorite, epidote, sericite, clay and ore occur as accessories. Plagioclase and quartz are coarse-grained and are enclosed by fine groundmass of quartz, feldspar, hornblende, chlorite, muscovite, biotite and ore. Quartz, plagioclase, perthite and hornblende are the primary minerals while epidote, chlorite, biotite and muscovite are secondary minerals formed by alteration of feldspar and amphibole.

3.2. Geochemistry

Twenty samples from the intermediate to felsic plutonic rocks exposed in the studied area were analyzed for major oxides and trace elements by using atomic absorption spectrometer and UV/ visible spectrophotometer, while three samples were analyzed by X-ray fluorescence for major and trace elements (Table1).

Table 1. Major and trace element chemistry of diorites and granodiorites from the Drosh area, Chitral

SAMPLE	KG10	KG11a	KG11b	KG13	KG189	KG196	GL133	GL135	GL141	GL144	GOG38	GR84	GR95	GR96	GR97
SiO_2	60.78	55.89	58.98	57.98	58.7	55.13	62.78	63.78	59.04	62.89	58.78	55.67	55.45	56.98	71.6
TiO_2	0.63	0.55	0.39	0.41	0.85	0.52	0.75	0.51	0.72	0.51	0.44	0.36	0.41	0.41	0.17
Al_2O_3	18.78	16.89	17.67	18.96	17.71	15.23	15.89	18.96	18.76	15.75	14.23	15.23	16.45	16.89	10.81
Fe_2O_3	2.69	3.46	3.53	3.3	7.22	5.17	5.56	5.03	5.46	5.31	3.79	5.88	2.98	2.98	2.08
MnO	0.04	0.05	0.05	0.06	0.06	0.11	0.05	0.14	0.13	0.17	0.05	0.12	0.09	0.09	0.04
MgO	1.72	6.88	2.11	3.12	3.13	3.79	3.36	2.36	3.69	1.66	1.97	3.17	5.53	5.53	1.44
CaO	6.64	5.14	4.88	8.76	2.61	5.96	4.07	6	7.69	8.17	4.88	4.69	8.69	8.69	3.52
Na_2O	2.84	1.52	1.06	0.26	0.37	3.02	3.02	0.26	2.4	0.57	4.31	2.78	2.33	2.33	4.78
K_2O	2.66	4.06	3.84	4.46	3.82	1.43	2.51	0.23	0.91	0.99	2.42	2.71	1.39	1.39	0.42
P_2O_5	0.1	0.02	0.2	0.2	0.15	0.57	0.17	0.16	0.15	0.12	0.54	0.3	0.14	0.14	0.04
LOI	1.63	6.32	6.86	2.14	5.37	8.45	2.42	2.15	0.99	2.94	7.5	8.34	4.93	4.6	5.11
Total	98.51	100.78	99.57	99.65	99.99	99.38	100.58	99.58	99.94	99.08	98.91	99.25	98.39	100	100.01
Trace elements (ppm)															
Nb	ND	ND	ND	ND	16	ND	ND	ND	ND	ND	ND	ND	2	ND	3
Zr	ND	ND	ND	ND	168	ND	ND	ND	ND	ND	ND	ND	31	ND	60
Y	ND	ND	ND	ND	30	ND	ND	ND	ND	ND	ND	ND	9	ND	-
Sr	ND	ND	ND	ND	88	ND	ND	ND	ND	ND	ND	ND	255	ND	156
Rb	ND	ND	ND	ND	205	ND	ND	ND	ND	ND	ND	ND	58	ND	20
Cu	69	157	157	98	122	34	276	245	119	140	47	208	209	135	418
Pb	58	42	42	276	36	43	29	34	32	41	71	41	32	40	34
Zn	74	153	65	85	78	47	63	78	69	130	71	49	64	162	51
Ni	37	52	55	125	101	42	85	45	28	23	39	44	16	54	-
Cr	49	43	43	29	188	71	27	54	63	21	42	58	60	41	15
V	ND	ND	ND	ND	202	ND	ND	ND	ND	ND	ND	ND	218	ND	56
Ba	ND	ND	ND	ND	364	ND	ND	ND	ND	ND	ND	ND	367	ND	580
CO	43	24	62	41	17	34	44	46	53	49	45	1	58	58	13
Th	ND	ND	ND	ND	14	ND	ND	ND	ND	ND	ND	ND	ND	ND	5
Sc	ND	ND	ND	ND	14	ND	ND	ND	ND	ND	ND	ND	32	ND	9
Ga	ND	ND	ND	ND	20	ND	ND	ND	ND	ND	ND	ND	8	ND	4
U	ND	ND	ND	ND	3	ND	ND	ND	ND	ND	ND	ND	ND	ND	1

ND= Not Determined

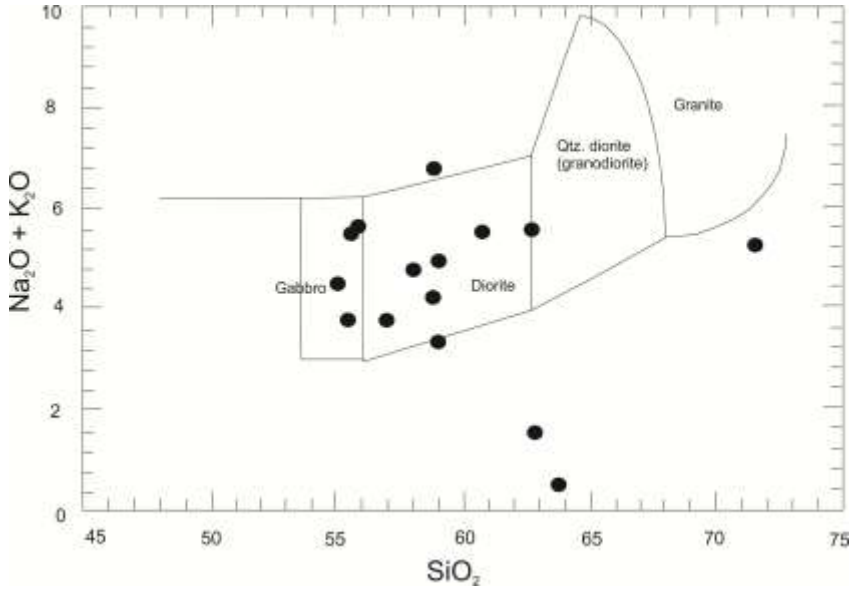

Fig. 2. Classification of the plutonic rocks intruding the Gawuch Formation using scheme of Cox et al. (1979) and Wilson et al. (1989).

The intermediate plutonic rocks of the studied area are classified using scheme of Cox et al. (1979) and Wilson (1989). According to this scheme (Fig. 2), the majority of the studied rocks classified as diorites. However, few samples plot outside the fields defined for diorite, which could be due to the low alkali contents caused by the leaching of alkalies (i.e. Na and K) during alteration process.

3.2.1. Major element chemistry

The diorites of the studied area are characterized by intermediate to high SiO_2 content (55-65 wt%), intermediate to low alkali content (<6 wt%), intermediate to high Al_2O_3 (avg. 16.6 wt%), and intermediate to low MgO content (1-7 wt%). These compositional characteristics suggest the parental magma of basaltic to andesitic composition. The studied diorites are metaluminous in characteristics, with the exception of three samples which are marginal between metaluminous and peraluminous (Fig. 3). The diorites are predominantly cal-alkaline (Fig. 4), although on the AFM diagram (Fig. 5), two of the analyzed samples have high FeO/MgO ratio. The studied diorites show great resemblance in major oxides with that of the Kohistan batholith (Petterson and Windley, 1986).

3.2.2. Trace element chemistry

The variation in the incompatible trace elements is shown in the form of spider diagram (Fig. 6). All the three representative samples have slopes inclined towards right indicating large-ion lithophile elements (LILE) enrichment (100 x primordial mantle) compared to high-field strength elements (HFSE). Two of the three samples show distinct negative anomaly for Nb. The same two samples are rich in Sr and low in Ti. It is clear from Figure 6 that the LIL elements show a broad scatter.

4. Tectonic setting of magma generation

In the major-element based Fe-Mg-Al diagram (Pearce et al., 1984) the studied diorites cluster closely in the combined field of Island arc and continental margin (Fig. 7 a). In the binary plot involving CaO and FeO+MgO (Fig. 7 b), all the studied diorites plot in the field covering island arc granitoids, calc-alkaline granitoids and collision-controlled granitoids. A similar tectonic setting is evident from a plot of FeOt/ (FeOt + MgO) vs. SiO_2 (Fig. 7 c). In the Ti-Zr-Y triangular diagram (Fig 7 d; Pearce and Cann, 1973), most of diorite samples fall in the fields defined for calc-alkaline basalt.

The high-aluminum or andesitic characteristics of the magma are clearly reflected in the composition of the analyzed diorites. Such magmas are typically produced in subduction-related settings particularly at continental margins (Wilson, 1989). The trace element chemistry such as the negative Nb anomaly, the enrichment of LILE relative to HFSE and the broader scattering of LILE is also suggesting the subduction related affinity for these diorites.

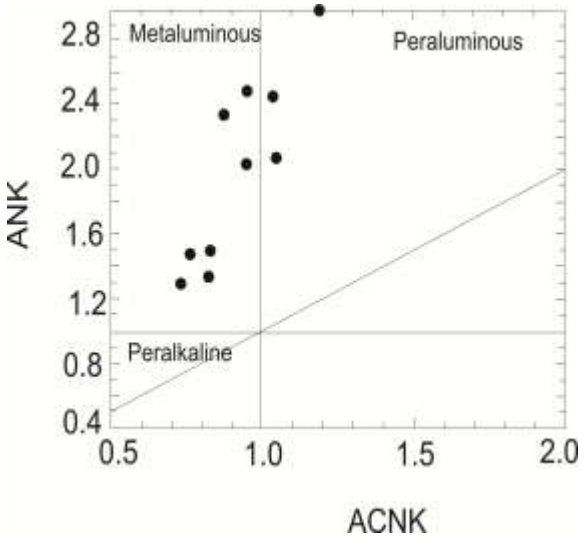

Fig. 3. Classification of diorites from the Gawuch Formation on the basis of Shands indices (after Maniar and Piccoli, 1989).

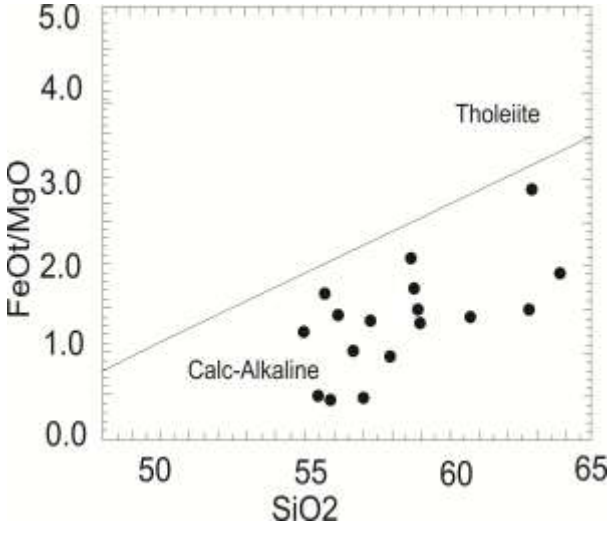

Fig. 4. SiO_2 versus FeO/MgO plot for diorites from the Gawuch Formation. The diagonal lines separates tholeiitic from calc-alkaline rocks (after Miyashiro, 1974).

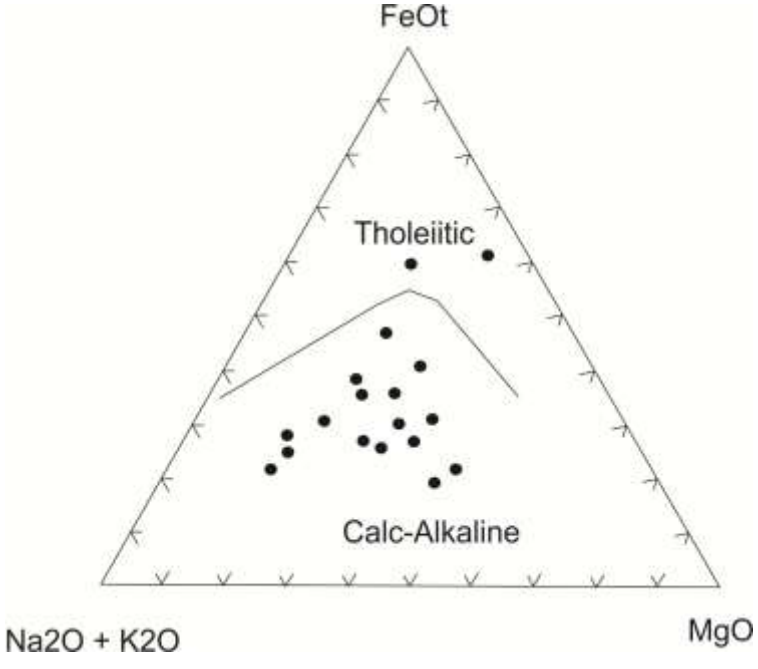

Fig. 5. AFM plot of Gawuch diorites. The line demarcating the division between calc-alkaline and Tholeiitic rocks after Irvine and Baragar (1971)

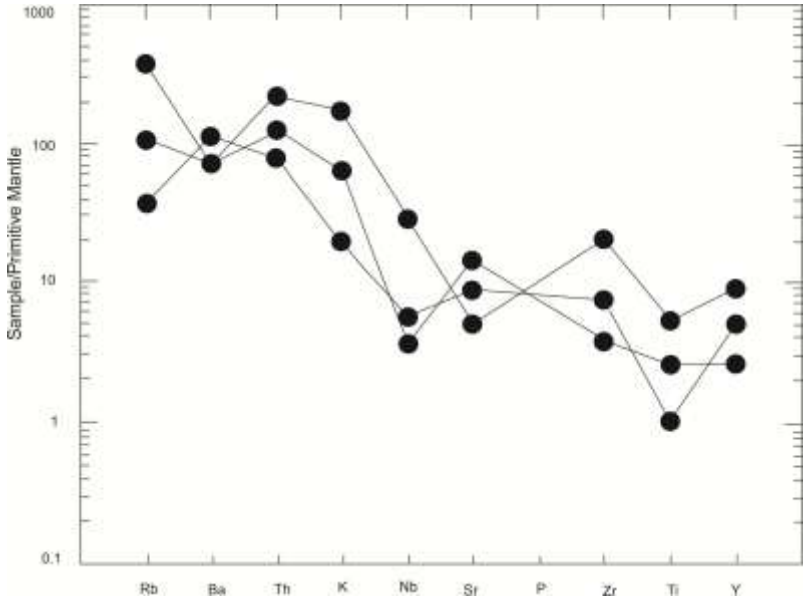

Fig. 6. Mantl-normalized spider diagrams for the trace elements of diorite rocks from the Gawuch Formation.

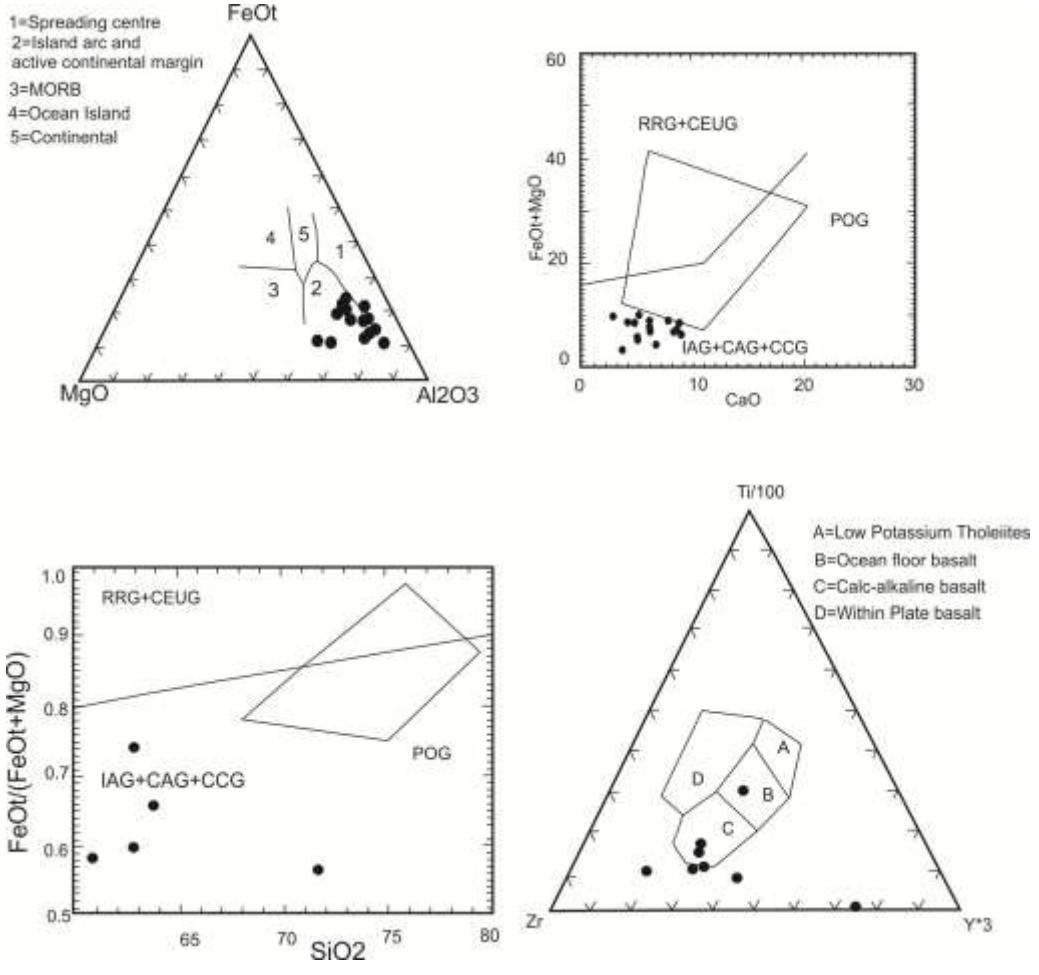

Fig. 7. Different discrimination diagrams showing the tectonic setting of diorites of the Gawuch Formation (Note that a subduction-related origin is indicated in all the diagrams used).

5. Copper mineralization

Four types of Copper mineralization based on field observations are observed in the area.

1) Copper mineralization along quartz veins.
2) Copper mineralization along foliation planes.
3) Disseminated Copper mineralization.
4) Supergene enrichment of Copper.

5.1. Copper mineralization along quartz veins

Numerous quartz veins along fractures and fissures intrude the rocks of the area. Most of these veins are enriched with copper-bearing sulfides and oxides, such as tetrahedrite, galena, chalcopyrite, pyrite, sphalerite and magnetite. These phases occur as coarse-grained irregular masses in the interstices between the quartz grains. Azurite and malachite occur mainly along the mineralized zone.

The textural characteristics of the silicate and ore phases in the quartz veins suggest that the ore phases precipitated along the interstices and fractures in the pre-existing quartz grains. This could be due to the later remobilization of the ore phases. At some places, the intergrowth textures between the various phases, especially tetrahedrite, galena, chalcopyrite and sphalerite suggest a simultaneous crystallization of these phases from the hydrothermal solutions. The textural feature suggested that chalcopyrite crystallized earlier than the rest of the ore phases. However, chalcopyrite inter-grown with the other ore phases (e.g., galena, sphalerite etc.) and in rare cases its presence as a fracture-filled material within in pyrite is suggesting several generations of its precipitation.

5.2. Copper mineralization along the foliation planes

Shearing along local faults is a common feature of the rocks in the study area. These shear zones are usually up to 5 m in thickness. The rocks in the shear zones are intensively fractured, mylonitized and schistose. Quartz and carbonate veining and the precipitation of the ore phases in these veins and also along the foliation planes is a common feature.

Copper mineralization in the form of tetrahedrite and chalcopyrite along with other sulfide phases like galena, sphalerite, chalcocite and pyrite are generally present along foliation planes in the zone of intense shearing. These ore phases are usually precipitated along foliation planes in the form of microveins or thin bands of carbonates and quartz. Complex secondary alteration of the copper-bearing phase is common in some areas. Primary chalcopyrite is altered to bornite and chalcocite, and secondary magnetite and limonite form bands around these sulfides. Where the rock is crenulated or has microfolds, the copper bearing phases are concentrated along the crests of the microfolds. This suggests that the mineralization in these rocks took place prior to the last phase of deformation.

5.3. Disseminated copper mineralization

Copper mineralization in the form of chalcopyrite and tetrahedrite occurs within the diorites. Chalcopyrite is the dominant phase and generally occurs as irregular grains within the interstices of silicate phases. At places the chalcopyrite has common intergrowth textures with tetrahedrite and sphalerite. Cubic grains of pyrite are also found in association with chalcopyrite and the tetrahedrite. Sphalerite forms irregular grains, occasionally found as intergrowth with chalcopyrite and also occurs in interconnected ameboidal masses. Tetrahedrite occurs as irregular masses associated with chalcopyrite and in some cases tetrahedrite replaces the chalcopyrite along the margins and fractures. Magnetite is fine- to medium-grained occurring as irregular grains and as fine-grained material disseminated throughout the rock. It is also present along the fractures and margins of chalcopyrite, Tetrahedrite and pyrite as replacement product and is mainly associated with limonite. Azurite, malachite, and limonite occur as alteration products, mostly along fractures and at the margins of sulfide phases.

5.4. Supergene enrichment of copper

Supergene enrichment of copper in the form of malachite and azurite is widespread along the sheared zones. The process of shearing and faulting significantly increased the penetration of ground water in to the ores resulting in oxidation of sulfide phase and hence malachite and azurite showings are commonly confined to shear zones. At places azurite also occurs as minute veinlet.

6. Ore mineralogy

6.1. Methodology

Identification of the ore minerals, in this study, is based on microscopic, electron microprobe and in some cases X-ray diffraction investigations. The electron microprobe analyses were performed on Cameca automated SX 50 Electron Microprobe at the University of South Carolina, USA. This machine is equipped with wavelength dispersive system (WDS) and an energy dispersive system (EDS). All the analyses were performed at 25Kv. Standards used were: pyrite, chalcopyrite, galena, sphalerite and tetrahedrite. All the Ore minerals were analyzed for Cu, Fe, Zn, Pb, As, Mn, Sb, S (Table 2).

The X-Ray Diffraction analyses were carried out on a Rigaku XRD at the NCE in Geology, University of Peshawar. The ore minerals observed in the mineralized zones are tetrahedrite, chalcopyrite, galena, pyrite, sphalerite, bornite and magnetite (Fig. 8).

The ore minerals in the mineralized quartz veins and associated mineralized diorites, granodiorites include tetrahedrite (5-60 vol. %), galena (5-20 vol. %), chalcopyrite (5-20 vol %), pyrite (5-15 vol %), magnetite (5-3 vol %), bornite (1-3 vol %), malachite (trace) and azurite (traces).

6.2. Tetrahedrite

Tetrahedrite is the most abundant copper-bearing phase, both in the quartz veins as well as in mineralized diorties. It occurs as a coarse-grained irregular mass, mostly filling the inter spaces of silicate phases and also along their fractures. Occasionally, tetrahedrite encloses the silicate phases, especially quartz. It is intimately associated with chalcopyrite and galena. At places tetrahedrite is highly fractured and is generally replaced by chalcocite and bornite along fractures. In some samples it appears to be replacing chalcopyrite too.

Electron microprobe analyses show the tetrahedrite to be stoichiometric $(CuFeZn)_{12}$ $(SbAs)_4$ S_{13}. Rim to core relationship in a single grain does not show any significant compositional variation (Table 2). Tetrahedrite shows less variations in Cu (40.10 to 42.84), Zn (5.35 to 6.89), S (25.25 to 27.33), Mg (0.11 to 0.32) and Fe (1.08 to 2.68). This suggests a homogenous nature of the Tetrahedrite whereas As (9.20 to 17.48) and Sb (5.23 to 17.51) have greater variation among different grains. The tetrahydride is also confirmed by XRD studies and pattern is shown in Figure 8a.

6.3. Galena

Galena appears in anhedral- to irregular-shaped patches having triangular pits on the surface. It is commonly intergrown with sphalerite, chalcopyrite and tetrahedrite, however, discrete grains with no intergrowths are also common. Galena is mostly precipitated within the interstices of silicate phases. At places galena exhibits textures reflecting strain. Rim to core analyses do not show any significant compositional variation suggesting a homogeneous nature of the grains. The electron microprobe analyses suggest galena to be nearly stoichiometric PbS (Table 2) containing traces of As (0.0 to 0.25), Sb (0.0 to 0.09), Fe (0.0 to 0.02), Ag (0.0 to 0.04) and Zn is below the detection limit. The galena is also confirmed by XRD studies and pattern is shown in Figure 8b.

6.4. Chalcopyrite

Chalcopyrite is the second most abundant copper-bearing phase in both the mineralized quartz veins and the mineralized diorites. It is white to brass-yellow in the reflected light and occurs as medium-grained irregular mass within the interstices of silicates. It generally occurs in three distinct forms: as medium-grained irregular masses, as intergrowth with tetrahedrite and galena, and as small blebs within sphalerite. At places, chalcopyrite and tetrahedrite enclose the silicate phases. In some sections tetrahedrite grains have chalcopyrite as a core material, suggesting that chalcopyrite could be the main primary phase which has been replaced by the tetrahedrite, Many chalcopyrite veinlets cut the pyrite grains indicating that some of the chalcopyrite was formed later than the bulk sulfide deposition. In some cases pyrite is replaced by chalcopyrite. In oxidized zones, chalcopyrite is extensively replaced by limonite, hematite and magnetite. Electron microprobe analyses show the chalcopyrite to be

stoichiometric $CuFeS_2$. Most of the analyses exhibit negligible or undetectable concentration of Pb and Sb, however, the other elements i.e. Zn (up to 0.05 Wt %), As (up to 0.12 wt%) and Ag (up to 0.08 wt%) have the detectable concentration in the chalcopyrite (Table 2). The chalcopyrite is also confirmed by XRD studies and pattern is shown in Figure 8c.

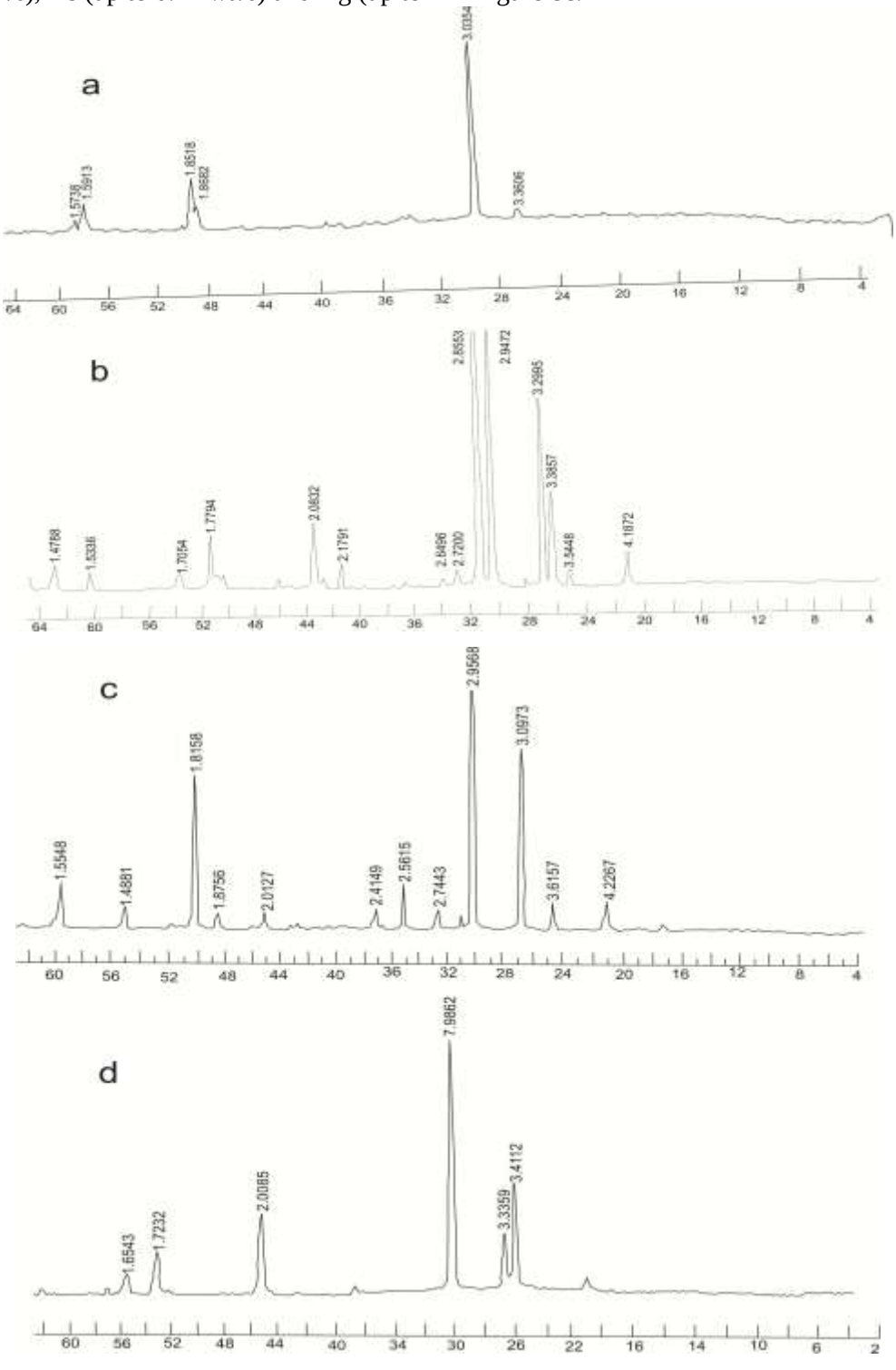

Fig. 8. (a) X Ray diffraction pattern of tetrahedrite from the Gawuch Formation.
(b) X Ray diffraction pattern of galena from the Gawuch Formation.
(c) X Ray diffraction pattern of chalcopyrite from Gawuch Formation.
(d) X Ray diffraction pattern of magnetite from Gawuch Formation

Table 2. Microprobe analyses of ore minerals from the Gawuch Formation, Drosh, Chitral.

TETRAHEDRITE

Sample	**GR 71**	**GR 71**	**GR 71**	**GR 71**	**GR 72**	**GR 72**	**GOG 19**	**GOG 19**	**GOG 19**	**GOG 19**	**GR 81**
Area	Rim	Core	Rim	Rim	Rim	Core	Rim	Core	Rim	Rim	Core
Cu	40.37	40.28	40.86	40.1	41.68	40.97	41.75	41.42	41.87	42.84	41.12
Zn	6.67	6.67	6.82	6.66	6.97	6.89	5.81	5.58	5.52	5.74	5.35
As	1051	9.27	9.2	6.86	12.21	10.74	15.73	15.03	16.82	17.48	10.66
Si	0	0	0	0	0	0	0	0	0	0	0
S	26.31	26.27	26.26	25.96	26.68	26.31	27.16	27.21	27.16	27.33	25.48
Pb	0	0	0	0	0	0	0	0	0	0	0
Ag	0.19	0.31	0.31	0.32	0.14	0.13	0.11	0.15	0.26	0.11	0.31
Sb	15.68	17.07	17.51	16.51	13.12	14.48	7.56	8.6	5.86	5.23	13.99
Mn	0	0.05	0	0.02	0	0	0	0	0	0	0
Fe	1.2	1.18	1.14	1.08	1.31	1.15	2.28	2.14	2.68	2.6	2.15
Total	100.94	101.11	102.09	100.5	102.1	100.67	100.13	100.13	100.16	101.32	99.05
Atomic Proportions											
Sum = 29											
Cu	9.96	9.97	10.05	9.99	10.06	10.08	9.99	9.96	9.99	10.09	10.3
Zn	1.6	1.61	1.63	1.61	1.64	1.65	1.35	1.31	1.28	1.31	1.3
As	2.2	1.95	1.92	2.08	2.5	2.24	3.19	3.07	3.4	3.49	2.26
S	1286	12.89	12.8	12.81	12.77	12.83	12.88	12.98	12.84	12.75	12.65
Sb	2.02	2.21	2.25	2.15	1.65	1.86	0.94	1.08	0.73	0.64	1.83
Fe	0.34	0.33	0.32	0.31	0.36	0.32	0.62	0.59	0.73	0.7	0.61

GALENA

Sample	**KG 225**	**KG 225**	**KG 225**	**KG 225**	**GOG 22**	**GOG 36**	**GOG 36**	**GOG 36**	**GL 54**	**GL 54**
Area	Rim	Core	Rim	Rim	Core	Rim	Core	Rime	Rime	Core
Cu	0	0	0	0	0	0	0	0	0	0
Zn	0	0	0	0	0	0	0	0	0	0
As	0	0.01	0	0	0.25	0	0	0	0.04	0
Si	0.1	0.02	0.11	0.18	0.12	0	0	0	0.12	0.12
S	12.38	12.88	12.2	12.89	12.2	13.36	13.35	12.68	12.55	12.23
Pb	86.37	86.09	86.97	86.85	86.34	87.53	86.09	85.34	86.78	86.76
Ag	0	0.01	0.04	0	0	0.01	0	0	0	0
Sb	0.04	0	0.06	0.03	0.08	0.09	0	0	0.01	0.01
Mn	0.02	0	0.02	0	0	0.02	0	0	0	0
Fe	0.02	0.02	0.01	0	0	0	0	0	0	0.02
Total	98.94	99.03	99.39	99.98	98.99	101.01	99.45	98.02	99.94	99.13
Atomic Proportions										
Sum = 2										
S	0.96	0.98	0.95	0.98	0.95	0.99	1	0.98	0.97	0.95
Pb	1.04	1.02	1.05	1.02	1.05	1.01	1	1.02	1.03	1.05

Table 2 (continued)

PYRITE

Sample	**KG 225**	**KG 225**	**KG 225**	**KG 225**	**GOG 36**	**GOG 36**	**GOG 36**	**GOG 26**	**GL 54**
Area	Rim	Core	Rim	Rim	Core	Rim	Rim	Core	Rim
Cu	0.06	0.08	0.06	0	0.05	0.05	0.08	1	0.25
Zn	0.05	0.05	0.08	0.01	0.06	0.05	0.04	0.03	0.03
As	0.04	0.04	0.05	0	0	0	0	0.01	0
Si	0	0	0	0	0	0	0	0	0
S	53.56	52.99	53.5	53.56	53.49	53.53	54.44	53	53.1
Pb	0	0	0	0	0	0	0	0	0
Ag	0	0	0	0	0	0	0	0	0
Sb	0	0	0	0	0	0	0	0	0
Mn	0	0	0	0	0	0	0	0	0
Fe	46.94	47	46.5	47.1	47.2	47.85	38.59	46.8	50
Total	100.65	100.16	100.19	100.67	100.8	101.48	93.15	100.84	103.38
Atomic Proportions									
Sum = 3									
S	1.99	1.98	2.12	2	1.95	1.98	2.13	1.99	1.95
Fe	1.01	1.02	0.88	1	1.05	1.02	0.87	1.01	1.05

CHALCOPHYRITE

Sample	**GR 72**	**GR 72**	**GOG 24**	**GOG 24**	**GOG 24**	**GR 81b**	**GR 81b**	**GR 81b**
Area	Rim	Core	Rim	Core	Rim	Rim	Core	Rim
Cu	35.04	34.81	33.05	33.5	33.06	35.73	35.26	35.07
Zn	0.05	0.04	0	0.05	0.04	0.05	0	0
As	0.07	0.06	0.05	0.02	0.05	0.04	0.12	0.08
S	34.8	35	34.75	34.75	34.1	39.97	34.87	34.92
Pb	0	0	0	0	0	0	0	0
Ag	0	0	0	0.08	0.08	0	0.02	0
Sb	0.01	0.02	0	0.03	0.01	0	0	0
Mn	0.02	0	0	0	0	0	0	0
Fe	30	29.89	30.29	31.09	31.09	30.04	30.28	30.28
Total	99.99	99.82	98.14	99.52	98.43	100.83	100.55	100.36
Atomic Proportions								
Sum = 4								
Cu	1.01	1.01	0.97	0.97	0.97	1.03	1.02	1.01
S	2	2.01	2.02	2	1.99	1.99	1.99	2
Fe	0.99	0.98	1.01	1.03	1.04	0.98	0.99	0.99

Table 2 (continued)

SPHELERITE

Sample	**KG225**	**KG225**	**KG225**	**GR 74**	**Gr 74**	**GR 74**	**GOG 37**	**GOG 37**
Area	Rim	Core	Rim	Rim	Core	Rim	Rim	Core
Cu	0.35	0.3	0.82	1	0.09	1	0.8	0.75
Zn	62.9	63.96	92.4	59	58.59	60.85	63.2	62.45
As	0.05	0.06	0.06	0.02	0.01	0	0.01	0.02
S	31.8	31.5	31.8	32	31.85	31.5	32.5	32.5
Pb	0	0	0	0	0	0	0	0
Ag	0	0	0	0	0	0	0	0
Sb	0.01	0.04	0.02	0.01	0.01	0	0.01	0
Mn	0	0	0	0	0	0	0	0
Fe	2.6	2.64	5.8	5.9	5.8	6	5.9	6
Total	97.71	98.5	100.9	97.93	96.36	99.35	102.42	101.72
Atomic Proportions								
Sum = 2								
Zn	0.96	0.97	0.93	0.9	0.9	0.92	0.93	0.92
S	0.99	0.98	0.97	0.99	1	0.97	0.97	0.98
FE	0.05	0.05	0.1	0.11	0.1	0.11	0.1	0.1
M%FeS	4.66	4.73	10.39	10.57	10.39	10.74	10.57	10.74

BORNITE

Sample	**GL 37**	**GL 37**	**GL 37**
Area	Rim	Core	Rim
Cu	61.89	62.78	63.24
Zn	0	0.09	0.05
As	0	0.06	0.09
S	26.12	25.98	25.65
Pb	0	0	0
Ag	0.17	0.04	0
Sb	0.07	0.03	0.02
Fe	11.48	11.3	11.67
Total	99.73	100.28	100.72
Atomic Proportions			
Sum = 10			
Cu	4.88	4.94	4.97
S	4.09	4.05	3.99
Fe	1.03	1.01	1.04

MAGNETITE

Sample	**Ps254**	**Ps254**	**Ps254**
Area	Rim	Core	Rim
Fe	72.36	71.9	73.36
O	27.64	26.64	23.06
Total	100	98.54	96.42
Atomic Proportions			
Sum = 2			
Fe	0.86	0.87	0.95
O	1.14	1.13	1.05

6.5. Sphalerite

Sphalerite is ameboidal in shape and is generally associated with or intergrown with galena and tetrahedrite. It is generally light brown in colour, however, reddish brown coloured grains are also noticed in few cases. Tiny (<1 micron size) disseminated blebs and rods of chalcopyrite within the sphalerite, termed as chalcopyrite disease, are also noticed. At places, iron staining along fractures, in association with light brown sphalerite is noticed. This can be attributed to the release of iron from sphalerite during oxidation.

The electron microprobe analyses suggest sphalerite to be stoichiometric ZnS (Table 2). Sphalerite is generally homogenous as rim to core relationships in single grain of sphalerite does not show any compositional variation (Table 2). The mole % of FeS in sphalerite ranges from 4.66 to 10.74 and is reflected in change in colour in the sphalerite grains from light-brown to reddish-brown, respectively.

Among the trace elements Cu is ranging from (0.09 to 1.00 wt%), As from (0-0.06 wt%) and Sb from (0 to 0.04 wt%), while the Pb and Ag are undetectable.

6.6. Pyrite

Pyrite is ubiquitous in all the sulfides-bearing phases. It has slightly high reflectivity and has white to light-yellow reflecting colors. Two distinct types of pyrites have been identified: 1) the early formed pyrite and 2) the later formed pyrite. The early formed pyrite has smooth surface and is generally present in anhedral, subhedral and rarely in euhedral form. The later formed pyrite (i.e. second generation) is mostly irregular in shape with some crystal outlines or partial crystal surfaces and is generally present along the microfractures of other sulfide and silicate phases.

Electron microprobe analyses suggest pyrite to be nearly stoichiometric FeS_2 (Table 2). Minor trace elements (i.e. Cu, As, Pb, Ag and Sb) have been analyzed. Most of pyrite analyses show negligible or undetectable concentration of these elements. However, Cu is present up to 1.0 wt%. Fe has wide range (38-50 wt%) whereas S has narrow range (53-55 wt%) in these pyrites.

6.7. Magnetite

It is of gray color with brownish tint and occurs as anhedral, subhedral and even in skeletal forms. It also occurs as anhedral polycrystalline aggregates. Irregular magnetite grains occur as interstitial phase, and enclose rounded to subrounded grains of silicate phases. It also occurs as micro veins along the foliation planes. Magnetite often contains exsolution or oxidation lamellae of hematite. It is mostly associated with pyrite, chalcopyrite, galena and sphalerite.

The electron microprobe analyses show the magnetite to be nearly stoichiometric Fe_3O_4. Most of the analyses exhibit negligible or undetectable concentration of Cu, Zn, Pb, and Ag. However, Fe has narrow range of variation (71.9 to 73.36 wt.%) and oxygen (23.06- 27.64 wt%) Table 2). The magnetite is also confirmed by XRD studies and pattern is shown in Figure 8d.

6.8. Bornite

Bornite occurs as irregular grains. It is generally found in association with tetrahedrite. However, in some samples it is also replacing tetrahedrite along the margins and fractures. Sometime it is intergrown with tetrahedrite and chalcopyrite.

Electron microprobe analyses show the bornite to be nearly Cu_5 Fe S_4 (Table 2). Traces of Zn (0.0 to 0.09 wt%), Ag (0.0 to 0.17 wt %) and Sb (0.02 to 0.07 wt%) are present. However, Pb is undetectable.

7. Chemical gain/loss accompanying mineralization

The hydrothermal mineralization is capable of greatly modifying the original chemical composition of the host rocks. The process involves addition of certain metallic elements to the original chemical composition. This may or may not necessarily involve removal of any element(s) from the protolith composition. However, since the chemical composition of rocks is expressed in wt%, the net effect is that rest of the elements have a comparatively lower percentage than prior to modification by the hydrothermal mineralization.

In order to determine the chemical changes during mineralization, mineralized diorites from four separate locations i.e. Kaldom Gol, Gawuch Gol, Gorin Gol and Langer Gol are compared with each other (Fig. 9) and also compared with unmineralized diorties collected from the same locations by computing the enrichment and depletion factors [(mineralized-unmineralized / unmineralized)*100] (Table 3). This involves assumption that the mineralized and unmineralized diorties had identical compositions prior to mineralization. Since there is no direct method to ascertain this requirement; care has been taken to select the mineralized and unmineralized diorites from the same body yet with a safe mutual distance to avoid any hydrothermal effect.

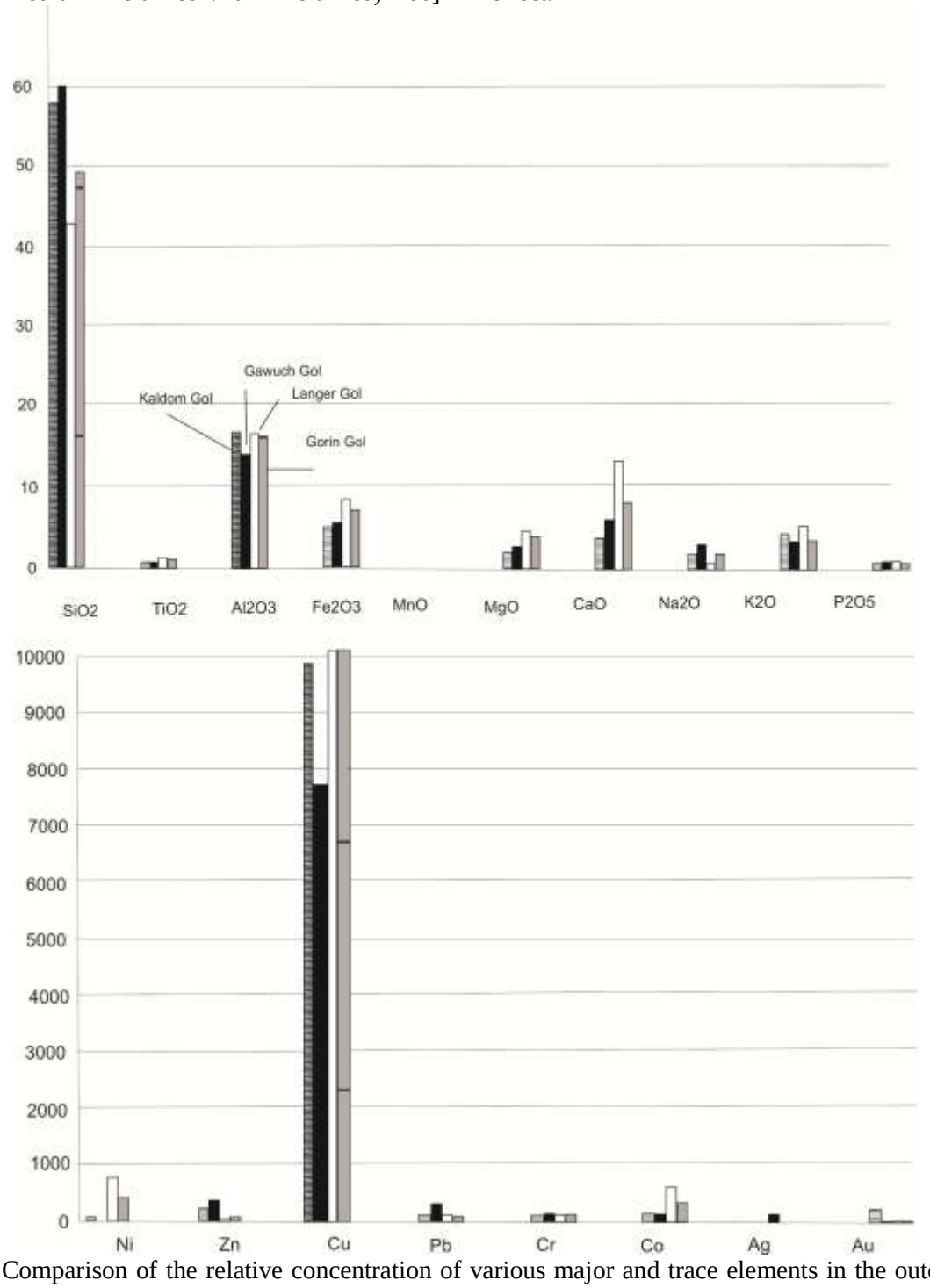

Fig. 9. Comparison of the relative concentration of various major and trace elements in the outcrops of the Gawuch Formation.

Table 3. Average major and trace element data of mineralized and unmineralized rocks from Gawuch Formation and their enrichment and depletion factors.

Kaldam Gol

Mineralized rocks

Samp. No	SiO_2	TiO_2	Al_2O_3	Fe_2O_3	MnO	MgO	CaO	Na_2O	K_2O	P_2O_5	Ni	Zn	Cu	Pb	Cr	Co	Ag	Au
KG 14	58.67	0.53	18.94	2.29	0.03	1.76	4.37	2.89	4.41	0.22	43	86	3408	42.22	53.4	54	0	10
KG 195	55.34	0.45	15.67	3.4	0.05	1.58	5.46	2.85	2.98	0.08	26	414	27525	137	30	37	0	0
KG 205	56.41	0.55	16.89	4.99	0.07	2.55	3.32	0.37	4.26	0.35	83	45	720	54	87	62	0	4
KG 209	60.89	0.63	15.34	9.38	0.12	0.58	0.33	0.4	3.14	0.63	59	288	7740	98	71	74	15	340
Average	57.83	0.54	16.71	5.02	0.07	1.62	3.37	1.63	3.7	0.32	53	208	9848	83	60	57	4	89

Unmineralized rocks

Samp. No	SiO_2	TiO_2	Al_2O_3	Fe_2O_3	MnO	MgO	CaO	Na_2O	K_2O	P_2O_5	Ni	Zn	Cu	Pb	Cr	Co	Ag	Au
KG 10	60.87	0.63	18.78	2.69	0.04	1.72	6.64	2.87	2.66	0.1	39	74	69	58	49	43	2	3
KG 11a	55.89	0.55	16.89	3.46	0.05	6.88	5.14	1.52	4.06	0.02	52	153	157	42	43	24	0	7
KG 11b	58.98	0.39	17.67	3.53	0.05	2.11	4.88	1.06	3.84	0.2	55	65	157	42	43	62	1	8
KG 13	58.98	0.39	17.67	3.53	0.05	2.11	4.88	1.06	3.84	0.2	55	65	157	42	43	62	0	7
KG 189	58.7	0.85	17.71	7.22	0.06	3.13	2.61	0.37	3.82	0.15	101	78	122	36	188	17	0	0
KG 196	55.13	0.52	15.23	5.17	0.11	3.79	5.96	3.02	1.43	0.57	42	47	34	43	71	34	0	0
Average	58.08	0.56	17.33	4.27	0.06	3.29	5.02	1.65	3.28	0.21	57	80	116	44	73	40	1	4

average data

	SiO_2	TiO_2	Al_2O_3	Fe_2O_3	MnO	MgO	CaO	Na_2O	K_2O	P_2O_5	Ni	Zn	Cu	Pb	Cr	Co	Ag	Au
Average Mineralized Rock	57.83	0.54	16.71	5.02	0.07	1.62	3.37	1.63	3.7	0.32	53	208	9848	83	60	57	4	89
Average Unmineralized Rock	58.08	0.56	17.33	4.27	0.06	3.29	5.02	1.65	3.28	0.21	57	80	116	44	73	40	1	4
Depletion/Enrichment Factor	-0.43	-2.7	-3.55	17.54	12.5	-50.84	-32.85	-1.06	12.9	54.84	-8	159	8385	88	-17	41	650	2024

Table 3. (Continued)

Gawuch Gol

Unmineralized Rocks

Samp. No	SiO_2	TiO_2	Al_2O_3	Fe_2O_3	MnO	MgO	CaO	Na_2O	K_2O	P_2O_5	Ni	Zn	Cu	Pb	Cr	Co	Ag	Au
GOG17	61.89	0.63	15.34	9.38	0.12	0.58	0.33	0.4	3.84	0.63	59	288	7740	98	71	74	64	15
GOG18	69.45	0.19	8.23	2.82	0.09	1.08	7.27	0.56	2.72	0.05	97	903	5475	67	48	41	0	18
GOG19	65.78	0.38	13.45	3.86	0.05	1.08	3.11	3	3.5	0.54	76	146	23700	208	58	73	38	58
GOG22	54.78	0.24	16.45	9.6	0.05	2.56	5.85	2.01	2.65	0.16	48	59	5370	39	45	85	0	18
GOG24	54.34	0.34	15.78	3.16	0.07	4.27	8.18	5.63	2.73	0.07	53	48	1035	36	98	59	35	10
GOG25	52.23	0.52	14..78	4.5	0.09	4.8	9.8	2.73	2.05	0.29	50	561	2655	924	108	41	0	22
Average	59.75	0.38	14.01	5.55	0.08	2.4	5.76	2.39	2.92	0.29	64	334	7663	229	71	62	23	24

Unmineralized Rocks

Samp. No	SiO_2	TiO_2	Al_2O_3	Fe_2O_3	MnO	MgO	CaO	Na_2O	K_2O	P_2O_5	Ni	Zn	Cu	Pb	Cr	Co	Ag	Au
GOG38	58.78	0.44	14.23	3.79	0.05	1.97	4.88	4.31	2.42	0.54	39	71	46.8	71	42	45	0	6

	SiO_2	TiO_2	Al_2O_3	Fe_2O_3	MnO	MgO	CaO	Na_2O	K_2O	P_2O_5	Ni	Zn	Cu	Pb	Cr	Co	Ag	Au
Average Mineralized Rock	59.75	0.38	14.01	5.55	0.08	2.4	5.76	2.39	2.9	0.29	64	334	7663	229	71	62	23	24
Average Unmineralized Rock	58.78	0.44	14.23	3.79	0.05	1.97	4.88	4.31	2.42	0.54	39	71	47	71	42	45	0	6
Depletion/Enrichment Factor	1.64	-12.88	-1.58	46.53	56.67	21.57	17.96	-44.59	19.83	-46.3	64	371	16273	22	70	38	0	292

Langer Gol

Mineralized Rocks

Samp. No	SiO_2	TiO_2	Al_2O_3	Fe_2O_3	MnO	MgO	CaO	Na_2O	K_2O	P_2O_5	Ni	Zn	Cu	Pb	Cr	Co	Ag	Au
GI57	42.7	1.1	16.5	8.3	0.1	4.1	12.9	0.3	4.8	0.5	753	24	48600	62	64	546	0	7

Unmineralized Rocks

Samp. No	SiO_2	TiO_2	Al_2O_3	Fe_2O_3	MnO	MgO	CaO	Na_2O	K_2O	P_2O_5	Ni	Zn	Cu	Pb	Cr	Co	Ag	Au
GI43	58.98	0.39	17.67	3.53	0.05	2.11	4.88	1.06	1.45	0.2	55	65	157	42	43	62	0	3
GI45	55.67	0.36	15.23	5.88	0.12	3.17	4.69	2.78	1.71	0.3	44	49	208	41	58	1	0	2
Average	57.3	0.4	16.5	4.7	0.1	2.6	4.8	1.9	1.6	0.3	50	57	183	42	51	31	0	3

	SiO_2	TiO_2	Al_2O_3	Fe_2O_3	MnO	MgO	CaO	Na_2O	K_2O	P_2O_5	Ni	Zn	Cu	Pb	Cr	Co	Ag	Au
Average Mineralized Rock	42.7	1.1	16.5	8.3	0.1	4.1	12.9	0.3	4.8	0.5	753	24	48600	62	64	546	0	7
Average Unmineralized Rock	57.3	0.4	16.5	4.7	0.1	2.6	4.8	1.9	1.6	0.3	50	57	183	42	51	31	0	6
Depletion/Enrichment Factor	-25.53	162.5	0	77.45	0	56.92	168.13	-84.74	200	50	0	-58	26516	49	26	1644	0	27

7.1. Kaldom Gol

An average of four mineralized diorites have been normalized against an average of five unmineralized diorites to assess the chemical gain and loss in the Kaldom Gol (Fig. 10). Amongst the major elements, SiO_2, TiO_2, Al_2O_3 and Na_2O show negligible difference between the mineralized and unmineralized diorties Fe_2O_3, MnO, K_2O and P_2O_5 are enriched in the mineralized rocks while MgO, and CaO are depleted. All the trace elements are enriched in the mineralized diorites relative to the unmineralized ones. However, the enrichment in the trace elements like Cu, Au and Ag is significant.

7.2. Gawuch Gol

The major elements in the average mineralized rock from the Gawuch Gol show enrichment in major elements like Fe_2O_3, MnO, MgO, CaO and K_2O and depletion in TiO_2, Al_2O_3, Na_2O and P_2O5. Like in the Kaldom Gol, all the trace elements show enrichment, particularly being significant in Cu. Enrichment in Ag and Au in the Gawuch Gol is not as significant as in the Kaldom Gol (Fig. 11).

7.3. Gorin Gol

At Gorin Gol, the mineralized diorites are enriched in major elements like TiO_2, Fe_2O_3, MnO, CaO, K_2O and P_2O_5 and are depleted in SiO_2, MgO and Na_2O (Fig. 12). Amongst the metallic trace elements, Cu is strongly enriched followed by Ni and Co.

7.4. Langer Gol

At Langer Gol, major elements like Al_2O_3 and MnO do not show any significant difference between the mineralized and unmineralized diorties, while TiO_2, Fe_2O_3, MgO, CaO, K_2O and P_2O_5 are enriched in the mineralized rocks and SiO_2, Na_2O are depleted (Fig. 13). In the trace elements, Cu mineralization is accompanied by enrichment in Co and Ni.

8. Discussion and conclusions

The behavior of major and trace elements in the mineralized diorites, suggests that the hydrothermal solution responsible for the copper mineralization has effected, to a very extent, the diorites of the area. Figures 10-13 represent chemical gain/loss budget for the entire mineralized zone. Amongst the major elements, Fe_2O_3, and K_2O are consistently enriched in the mineralized rocks from all the four sections i.e. Kaldom Gol, Gawuch Gol, Langer Gol and Gorin Gol, while Na_2O is consistently depleted everywhere in the mineralized diorties compared to the unmineralized diorites. P_2O_5 and MnO show considerable enrichment in the mineralized diorties everywhere except for the P_2O_5 in Gawuch Gol and MnO in Langer Gol suggesting that it formed an important component of the mineralizing fluids. SiO_2 has either remained unchanged or only slightly depleted compared to the unmineralized diorites. Similarly Al_2O_3 has not been added or removed from the mineralized diorites to a great extent. TiO_2, CaO and MgO show anomalous behavior. Amongst the trace elements, Cu is strongly enriched everywhere in the mineralized rocks. None of the rest of the trace elements analyzed show depletion in the mineralized diorites relative to the unmineralized diorites.

Geochemical data, involving both major and trace elements have been used to characterize the petrology and tectonic setting of the igneous rocks of the area. Metavolcanic rocks belonging to Gawuch Formation are calc-alkaline in nature and detailed treatment in terms of mantle-normalized trace element patterns and discrimination diagrams involving immobile trace elements, however, suggest that these volcanics were originated with a strong subduction component (Tahirkheli et al., 2005). The suite of analyzed diorites is calc-alkaline in its petrology and contains strong subduction component. Since the diorites of the study area are probably related with the pluton at Lowari Pass, for which an age of 40-45Ma is available (Zeitler et al., 1982), a continental margin tectonic setting of origin can be assigned to the diorites of the study area.

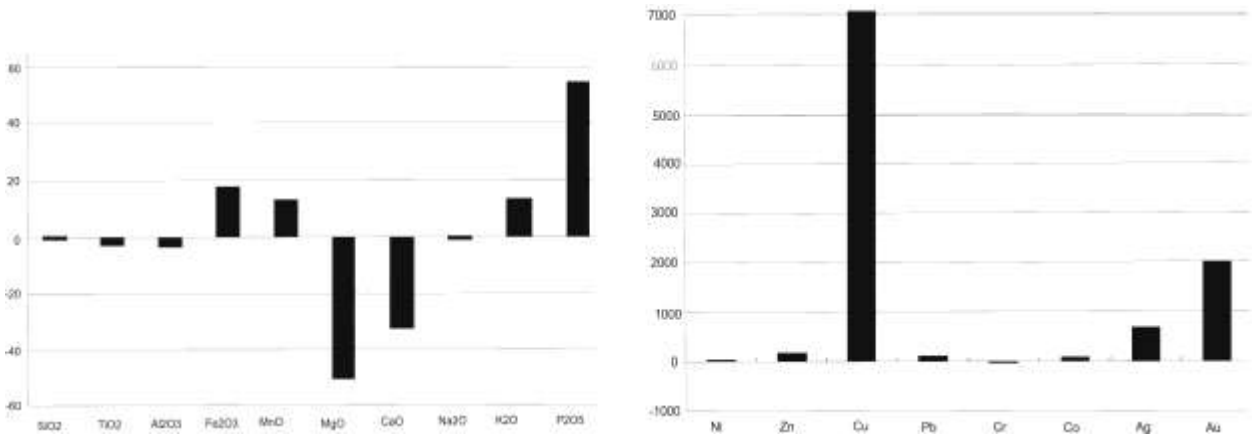

Fig. 10. Enrichment and depletion in major and trace element abundances in mineralized rocks in the Gawuch Formation exposed at the Kaldom Gol during alteration and mineralization.

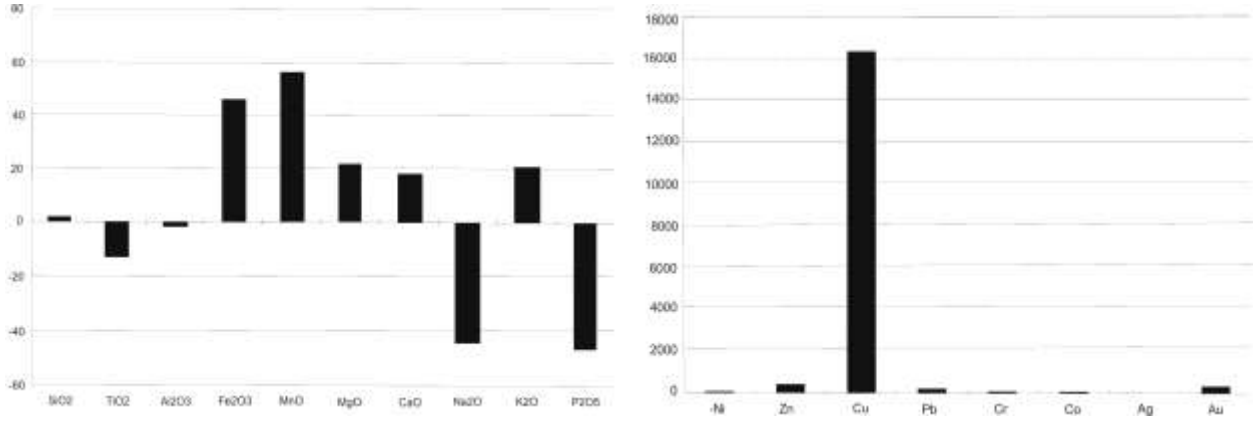

Fig. 11. Enrichment and depletion in major and trace element abundances during alteration and mineralization of diorites in the outcrops of Gawuch Formation at Gawuch Gol.

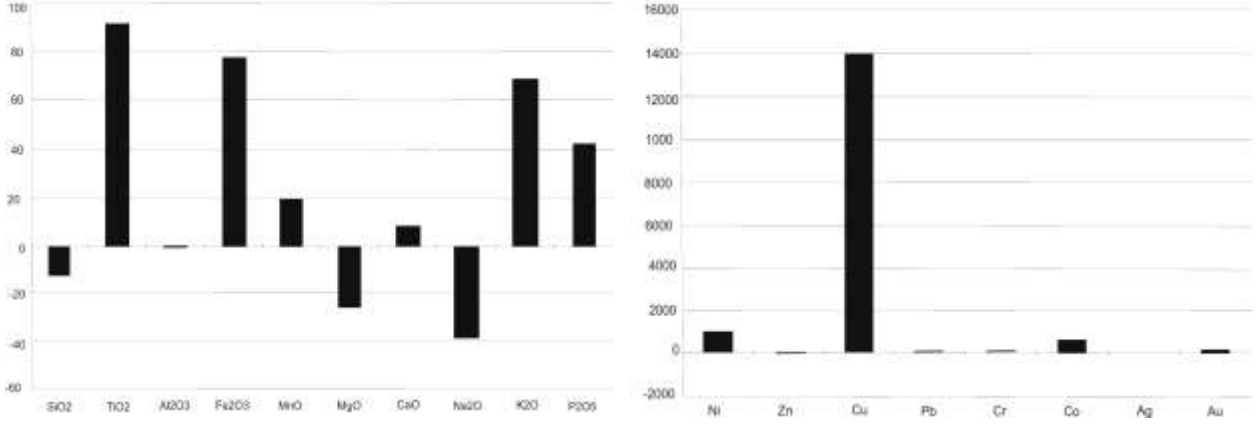

Fig. 12. Enrichment and depletion in major and trace element abundances during alteration and mineralization of diorites from Gawuch Formation exposed at Gorin Gol.

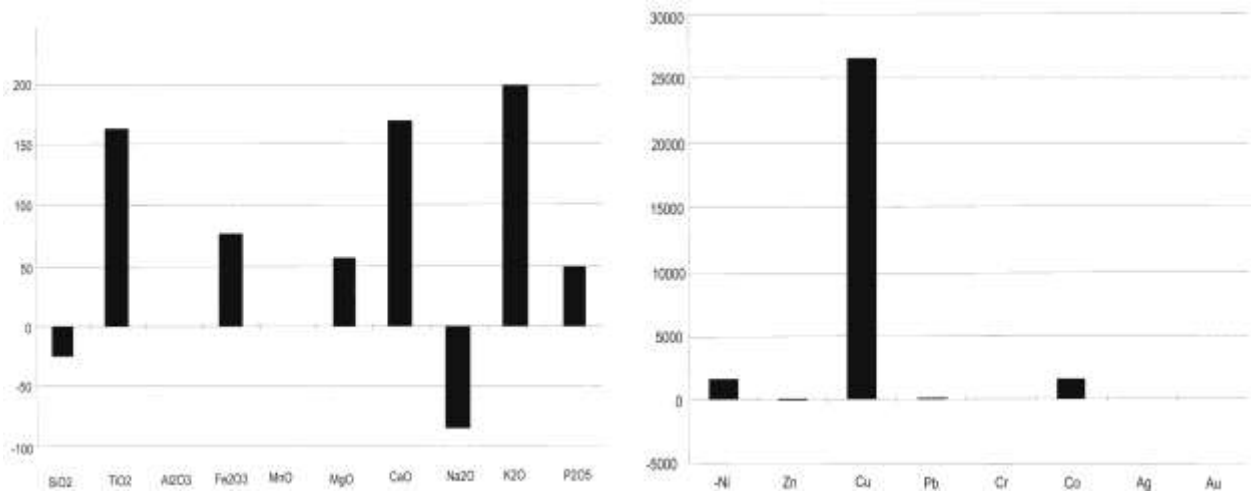

Fig. 13. Enrichment and depletion in major and trace element abundances during alteration and mineralization of diorites from Gawuch Formation exposed at Langer Gol.

As the Rocks of the area have been metamorphosed to greenschist- and at places, to epidote-amphibole facies metamorphism, these rocks have well developed fabrics, faulting and shearing. The Cu mineralization occurs within the diorite sills, dikes and plugs, suggesting the involvement of either magmatic or metamorphic water for Cu mineralization in Gawuch Formation. Tahirkheli et al. (1998) on the basis of $\delta^{18}O$ values of the quartz in the quartz veins and the mineralizing fluid have suggested the involvement of the magmatic fluid rather than metamorphic fluid for the studied cu mineralization.

Several lines of investigations have been adopted to ascertain the nature and petrogenesis of copper mineralization in study area including field observation, petrography, geochemistry, mineral chemistry and measurement of isotope ratio of Pb in galena (Tahirkheli et al., 2005) and oxygen in quartz veins (Tahirkheli et al., 1998). The principal attributes constraining the nature and origin of the studied mineralization include: 1) the mineralization is spatially restricted to narrow belt of width of 5-45m, 2) the locale of mineralization is controlled by stratigraphy (i.e. it is confined to upper part of Gawuch Formation) and is associated with diorites and granodiorite sills intruding upper part of the formation. It may be noted that the basal part of Gawuch Formation, immediately adjacent to Lowari pluton is devoid of mineralization. 3) The stratigraphic control, confining the mineralization to the upper parts of the Gawuch Formation is further controlled by presence of impervious lithology of Purit Formation on the top of the Gawuch Formation. The red shale of the Purit Formation serve as a cap rock sealing the upper migration of the hydrothermal solution from the upper part of the Gawuch Formation, resulting in their entrapment and concentration at this stratigraphic locale and 4) the presence of fractures and fissures, commonly associated with mineralization, together with presence of quartz veining imply a structural control on studied mineralization.

These attributes derived from geological field observation, point to hydrothermal origin for mineralization in Drosh–Shishi area. The close association with diorites-granodiorite minor intrusion suggests that the primary source for the solution responsible for mineralization rests with igneous intrusion rather than with volcanics.

Results from the fluid inclusion studies (Tahirkheli et al., 1997) combined with Oxygen isotope studies (Tahirkheli et al., 1998) show a high $\delta^{18}O$ signature ($\delta^{18}O$ isotopic composition of 5.79-9.62 per mil, with mean value of 7.98 per mil). This suggests the involvement of isotopically heavy ore forming fluid, in the alteration and copper mineralization in diorites and quartz veins (Tahirkheli et al., 1998).

The presence of igneous activity in the form of diorite-granodioritic plugs, sills and dykes (as apophyses of the Lowari pluton) hosting the mineralization suggest a role of magma in the generation of hydrothermal system rather than metamorphism. It is, therefore, hypothesized that the diorite-granodiortie plutons existing at depth beneath the mineralization could have been sources of brine metalliferous fluids. These fluids have precipitated the Cu-sulfide phases along silica mainly in the form of quartz vein in shallow level.

The age of the studied mineralization in Drosh-Shishi area remains to be fully understood. The geological evidence relating to mineralization with Kohistan batholiths points to an early Tertiary age i.e. same as that of the Lowari pluton (Zeitler et al., 1982).

9. Conclusions

The diroretic intrusions within the Gawuch Formation are of calc-alkaline nature having strong subduction related component. The hydrothermal activity related to the dioritic intrusion is responsible for the sulfide mineralization in the form of tetrahedrite, chalcopyrite, sphalerite and galena in the Gawuch Formation of the Drosh-shishi area.

Acknowledgement

We are very thankful to the Director NCE in Geology, University of Peshawar for providing the financial assistance and laboratory facilities.

References

Bard, J.P., Maluski, H., Matte, P.H., Proust, F., 1980. The Kohistan sequence; Crust and mantle of an obducted island arc. Geological Bulletin University of Peshawar, 13, 87-94.

Cox, K.G., Bell, J.D., Pankhurst, R.J., 1979. The interpretation of igneous rocks. Allen and Unwin, London.

Irvine, T.N., Baragar, W.R.A., 1971. A guide to the chemical classification of the common volcanic rocks. Canadian Journal of Sciences, 8, 523-548.

Khan, M.A., Jan, M.Q., Windley, B.F., Tarney, J., Thirlwall, M.F., 1989. The Chilas mafic-ultramafic igneous complex; the root of the Kohistan island arc in the Himalaya of northern Pakistan. Geological Society of America, Special Paper. 232, 75-94.

Khan, T., Khan, M.A., Jan, M.Q., 1994. Geology of a part of the Kohistan terrain between Gilgit and Chilas, Northern Areas, Pakistan. Geological Bulletin University of Peshawar, 27, 99-112.

Maniar, P.D., Piccoli, P.M., 1989. Tectonic discrimination of granitoids. Bulletin Geological Society of America, 101, 635-643.

Miyashiro, A., 1974. Volcanic rock series in island arc and active continental margins. American Journal of Sciences, 274, 321-355.

Pearce, J.A., Cann, J.R., 1973. Tectonic setting of basic volcanic rocks determined using trace element analyses. Earth and Planetary Science Letters, 19, 290-300.

Pearce, J.A., Harris, N.B.W., Tindle, A.G., 1984. Trace element discrimination diagrams for tectonic interpretation of Granitic rocks. Journal of Petrology, 25, 956-983.

Petterson, M.G., Windley, B.F., 1986. Petrological and Geochemical evolution of the Kohistan arc-batholith, Gilgit, N. Pakistan. Geological Bulletin University of Peshawar, 19, 121-149.

Petterson, M.G., Windley, B.F., 1991. Changing source regions of magmas and crustal growth in the Trans-Himalayas: Evidence from the Chalt volcanics and Kohistan batholith, Kohistan, northern Pakistan. Earth and Planetary Science Letters, 102, 326-341.

Pudsey, C.J., Coward, M.P., Luff, I.W., Shackleton, R.M., Windley, B.F., Jan, M.Q., 1985. Collision zone between the Kohistan arc and the Asian plate in NW Pakistan. Transactions of the Royal Society of Edinburgh, Earth Sciences, 76, 463-479.

Pudsey, C.J., Maguire, P.K.H., 1986. Magnetic profiles across the northern suture, Kohistan, NW Pakistan. Geological Bulletin University of Peshawar, 19, 47-60.

Shah, M.T., Shervais, J.W., 1999. The Dir-Utror metavolcanic sequence, Kohistan arc terrane, northern Pakistan. Journal of Asian Earth Sciences, 17, 459-475.

Tahirkheli, R.A.K., Jan, M.Q., 1979. A preliminary geological map of Kohistan and the adjoining areas, N. Pakistan. Geological Bulletin University of Peshawar, 11, (in pocket).

Tahirkheli, T., Khan, M.A., Shah, M.T., 2005. Geochemistry and petrogenesis of metavolcanic rocks in Gawuch and Drosh formations, Chitral, northern Pakistan. Geological Bulletin University of Peshawar, 38, 189-202.

Tahirkheli, T., Shah, M.T., Khan, M.A, 1998. Oxygen Isotope signature of the hydrothermal copper mineralization in Drosh-Shishi area, Chitral, Pakistan. Acta Mineralogica Pakistanica, 9, 111-116.

Tahirkheli, T., Shah, M.T., Khan, M.A., 1997. Mineralogical, Isotopic and fluid inclusion studies of the hydrothermal copper mineralization in Drosh- Shishi area, Chitral, Pakistan. Proceedings of National Symposium on economic geology of Pakistan, Islamabad, 59-71.

Wilson, M., 1989. Igneous Petrogenesis, A Global Tectonic Approach. London Unwin Hyman.

Zeitler, P.K., Johnson, N.M., Naseser, G.W., Tahirkheli, R.A.K., 1982. Fission-Track evidence for quaternary uplift of the Nanga Parbat region, Pakistan. Nature, 298, 255-257.